Weierstraß-Institut
für Angewandte Analysis und Stochastik

im Forschungsverbund Berlin e.V.
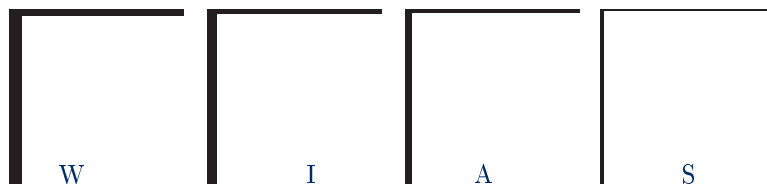
Linear Stability of a Ridge

J. R. King [3], A. Münch [1,2], B. Wagner [1]

submitted: November 16, 2005

[1]   Weierstrass Institute for Applied Analysis and Stochastics
      Mohrenstrasse 39
      10117 Berlin, Germany
      E-Mail: wagnerb@wias-berlin.de
[2]   Institute of Mathematics
      Humboldt University
      10099 Berlin, Germany
      E-Mail: muench@mathematik.hu-berlin.de
[3]   Theoretical Mechanics Section,
      School of Mathematical Sciences
      University of Nottingham
      Nottingham NG7 2RD, UK
      E-Mail: John.King@nottingham.ac.uk

No. 1070

Berlin 2005

W   I   A   S

Abstract

We investigate the stability of the three-phase contact-line of a thin liquid ridge on a hydrophobic substrate for flow driven by surface tension and van der Waals forces. We study the role of slippage in the emerging instability at the three-phase contact-line by comparing the lubrication models for no-slip and slip-dominated conditions at the liquid/substrate interface.

For both cases we derive a sharp-interface model via matched asymptotic expansions and derive the eigenvalues from a linear stability analysis of the respective reduced models. We compare our asymptotic results with the eigenvalues obtained numerically for the full lubrication models.

1   Introduction

Contact-line instabilities for thin liquid films that wet a solid substrate have been studied for decades, both theoretically and experimentally. The instabilities are typically driven by forces such as gravity [1, 2, 3, 4], Marangoni stresses or both [5, 6, 7, 8, 9]. The derivation of reduced mathematical models exploits the separation of length scales to obtain a simplified lubrication model from the underlying Stokes equations in conjunction with conservation of mass. The stress singularity at the three-phase contact line, which is inherited by the resulting fourth-order partial differential equations, is regularized for example via a slip boundary condition or a precursor model, where the height of the precursor or the slip length are usually much smaller than the height of the actual wetting film. The choice of the boundary condition at the three phase contact line typically enters only weakly in that it is believed that it does not significantly influence the eventual appearance of fingers; see for example [3, 8, 10, 11].

Compared to the wetting scenarios, the film thickness in dewetting experiments is typically orders of magnitude smaller. The physical situation on which we focus here consists of a thin viscous polymer film that is uniformly spread on a

substrate such as a silicon wafer with a hydrophobic coating. For such a multi-layered system one can reconstruct the disjoining pressure from a corresponding intermolecular potential which is composed of attractive long-range van der Waals contributions and a short-range term which accounts for Born-type repulsion, see e.g. [12, 13]. The latter term provides a cut-off by penalizing a thinning of the film below a positive thickness threshold given by the minimum of the potential. In such a situation the thin film dewets in a process that is initiated either spontaneously through spinodal decomposition or is induced, for example through nucleation. The dry spots, or holes, that form as a result subsequently grow as the newly-formed contact line recedes, thereby accumulating liquid in a characteristic capillary ridge at the edge of the hole, which increases in width and height as the dewetting proceeds. In a variety of experimental situations it is observed that, while in some cases the growth of the hole continues until it collides with neighboring holes, in others the ridge of the hole destabilizes into finger-like structures, eventually pinching off to form droplets. Such finger-like contact-line instabilities have also been observed for straight (as opposed to radially-symmetric) dewetting fronts; see [14, 15, 16, 17, 18, 19, 20]. Because of the impact this has on the emerging macroscopic pattern, it is important to understand the dynamics leading to such an instability.

For such situations, the relevance for the instability of slippage at the liquid/solid interface has been discussed by several authors, [21, 22, 23, 24, 25]. In [26, 27, 28] the dewetting rate and shape of the ridge have been treated using approximate formulas derived from scaling arguments and energy balances. In comparison to wetting phenomena, however, contact-line instabilities for dewetting thin films in the context of lubrication theory have received much more limited attention.

In order to capture the dynamics of the contact-line instability it is convenient to describe the evolution of the film surface $z = h(x, y, t)$ via a lubrication approximation that includes the influence of surface tension and the intermolecular potential $\phi(h)$ of the air/liquid/solid layer. Coordinates have been introduced here so that x, y denote directions parallel to the (planar) substrate and z the direction normal to it. In this case the pressure at $z = h(x, y, t)$ is given to leading order in the thin-film approximation by

$$p = -\Delta h + \phi'(h). \tag{1.1}$$

where $\phi'(h)$ is the first derivative of the intermolecular potential with respect to the liquid film thickness h. A typical choice for $\phi(h)$, and the one we will adopt

2

in this paper, is [12]

$$\phi'(h) = \varepsilon^{-1}\Phi'(h/\varepsilon), \quad \text{where} \quad \Phi(v) = \frac{1}{8v^8} - \frac{1}{2v^2}. \tag{1.2}$$

Note that $\Phi'(1) = 0$ and $\Phi''(1) > 0$, so that ϕ has a minimum at $h = \varepsilon \ll 1$; the reason for incorporating the dependencies upon ε embodied by (1.2) will become clear in sections 3 and 4. This implies that very thin films with a thickness scale of ε are energetically preferred to, in particular, thicker films, and the latter therefore tend to dewet. Making use of the length-scale separation in the x, y vs. z directions, one can then derive the lubrication model [29] from the Stokes equations and (1.1), namely

$$h_t + \nabla \cdot [h^n \nabla (\Delta h - \phi'(h))] = 0, \tag{1.3}$$

stated here (as are all equations in this paper) in non-dimensional form. Here h^n is the mobility coefficient, where the power n depends on the boundary conditions at the liquid/solid interface. A widely used condition relates the slippage velocity u of the liquid at the wall to the local shear rate u_z via

$$u = b\, u_z \quad \text{at} \quad z = 0, \tag{1.4}$$

where the slip length β is defined as the distance below the substrate at which the liquid velocity extrapolates to zero. For the above slip boundary condition, the no-slip condition is obtained if $b = 0$. On the other hand, for large b one can show [24], [25] that the mobility is h^2. In [24] a linear stability analysis showed that small perturbations of the receding front are amplified, and by orders of magnitude larger in the slip-dominated case than in the no-slip one. Moreover, while the perturbations of the contour lines become very symmetrical with respect to the maximum of the ridge in the no-slip case, they are asymmetrical in the slip-dominated regime and in [30] it was shown via numerical simulations that these properties carry over into the nonlinear dynamics of the perturbations. In the context of lubrication models for dewetting shear-thickening liquids, [31] derived asymptotic solutions for the shape of the dewetting ridges, their dewetting rates and their contact-line instability via matched asymptotic expansions. In [32] a variational formulation was used to obtain a free boundary problem for the contact line for the no-slip situation, and a stability analysis of the contact-line motion was performed in [33].

The purpose of this paper is study the role of slippage on the instability of the three-phase contact line by comparing linear stability results for the lubrication

models with mobilities h^3 and h^2. We pursue this by considering the simplest situation of the evolution of a perturbed stationary ridge. For this problem we first derive sharp-interface models for the lubrication models via matched asymptotic expansions. The resulting reduced models turn out to be simple enough to enable in some cases the derivation of the dispersion relation analytically and they allow good – and for the slip-dominated case even excellent – comparison with our numerical results.

We begin our analysis by first studying the stability of the ridge numerically in section 2. In section 3 and 4 we derive the sharp-interface models and the corresponding dispersion relations and compare them to our numerical findings.

2 Stationary ridges and their stability

In this section we study numerically the contact-line instability of a stationary ridge that initially extends to $\pm\infty$ in the y-direction, and is symmetrical about zero in the x-direction, and assumes the (small) equilibrium height εh_∞ for $x \to \pm\infty$. We thus begin with the lubrication model (1.3), (1.2), together with the boundary conditions

$$\lim_{x \to \pm\infty} h(x, y, t) = \varepsilon h_\infty. \tag{2.1}$$

From (1.3), (2.1), the ridge profiles can readily be found by dropping all terms with derivatives in t and y and integrating the resulting ODE. The constants of integration are determined by the far-field conditions, and we obtain, after two integrations,

$$h_x = \pm 2^{1/2} \left[\phi(h) - \phi(\varepsilon h_\infty) - \phi'(\varepsilon h_\infty)(h - \varepsilon h_\infty)\right]^{1/2}. \tag{2.2}$$

The plus sign applies for the left side of the ridge and the minus sign for the right. We assume in our scalings that the cross-sectional area of the fluid in the ridge is such that its maximum is one (without losing generality, since this can always be achieved by rescaling the equation with $h_{\max}$ and redefining ε). This assumption implies that the right-hand side of (2.2) must be zero for $h = 1$, i.e. we must observe the constraint

$$\phi(1) - \phi(\varepsilon h_\infty) - \phi'(\varepsilon h_\infty)(1 - \varepsilon h_\infty) = 0. \tag{2.3}$$

This fixes h_∞ for a given ε (on which ϕ depends). One easily finds for (1.2) that $h_\infty \sim 1 + \varepsilon/16$ as $\varepsilon \to 0$. Note that $h_\infty = 1 + O(\varepsilon)$ holds more generally as long

as $\phi'(\varepsilon) = 0$. Profiles for the ridges for different values of ε are shown in figure 1; note that the base states do not depend on the mobility h^n, and hence are the same for the no-slip and the slip cases.

Next we probe the stability of these equilibrium solutions with respect to disturbances in the y-direction via the normal modes ansatz

$$h(x, y, t) = h_0(x) + \beta h_1(x; k)e^{iky+\sigma t}, \qquad \text{where} \quad 0 < \beta \ll 1,$$

and $h_0(x)$ is the previously-found ridge profile. Introducing this into (1.3) and (2.1) we obtain the $O(\beta)$ problem

$$\begin{aligned} \sigma h_1 + \partial_x \left[h_0^n \partial_x \left(h_{1xx} - k^2 h_1 - \phi''(h_0)h_1 \right) \right] \\ -k^2 h_0^n \left(h_{1xx} - k^2 h_1 - \phi''(h_0)h_1 \right) = 0 \end{aligned} \qquad , \quad (2.4)$$

and

$$\lim_{x \to \pm \infty} h_1(x; k) = 0. \tag{2.5}$$

The eigenvalue problem (2.4), (2.5) was solved on a sufficiently large, finite domain using a standard finite-difference discretization scheme and inverse vector iteration to calculate the two eigenvalues with the largest real part, for a range of wavenumbers k. It turns out that both eigenvalues are real. One is negative for all $k > 0$ while the other is positive for all nonzero wave-numbers below a certain cut-off value k_c, and negative $k > k_c$. This unstable one is a peristaltic mode, whereby the sinusoidal perturbations of the contact lines on each side of the ridge are out of phase by half a wavelength. The other, i.e. stable, eigenvalue corresponds to perturbations that are in phase, i.e. are zig-zag modes. Details of the results can be found in figure 2 for the peristaltic and figure 3 for the zig-zag mode. Note that the eigenvalues do (of course) depend on the mobility, i.e. on the value of n. In figure 2 the wavelength of the unstable mode and its growth rate are slightly larger for the slip than for the no-slip case, while the cut-off (neutrally-stable) wavenumbers k_c are quite close. The difference is even more dramatic for the zig-zag mode, where the eigenvalue for the slip case is about twice that for no-slip.
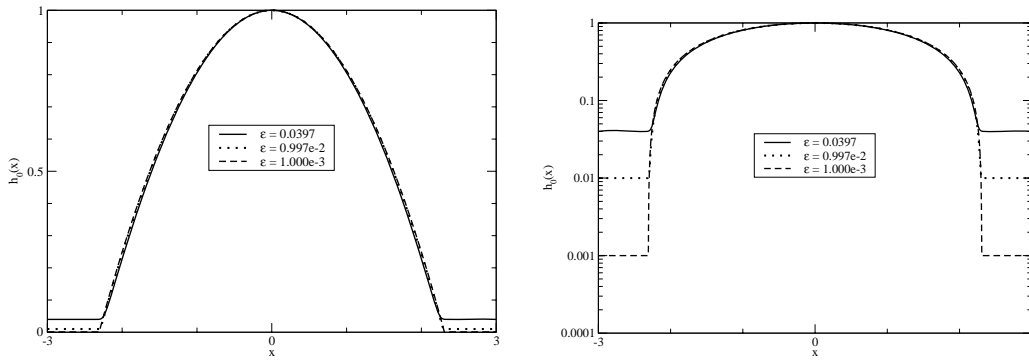
Figure 1: The ridge profiles for different values of ε. On the right side, the axis for h_0 has been scaled logarithmically to enlarge the thin profiles beyond the 'contact lines'.
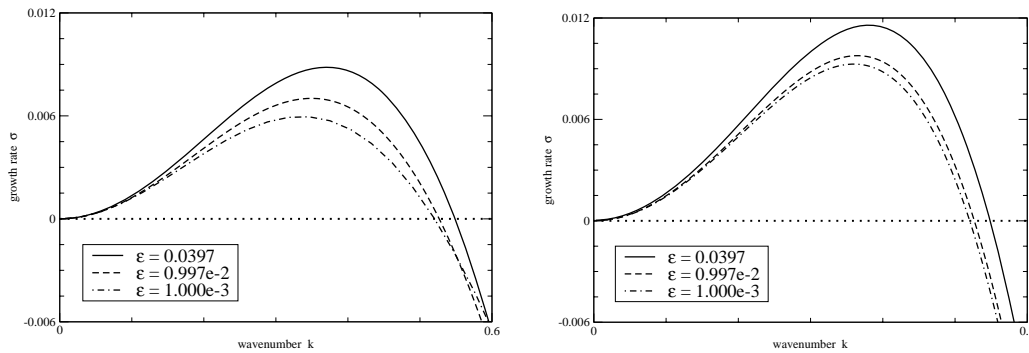

Figure 2: The growth rates for the (unstable for $0 < k < k_c$) peristaltic mode for different values of ε, for the no-slip case $n = 3$ (left) and for the slip case $n = 2$ (right).
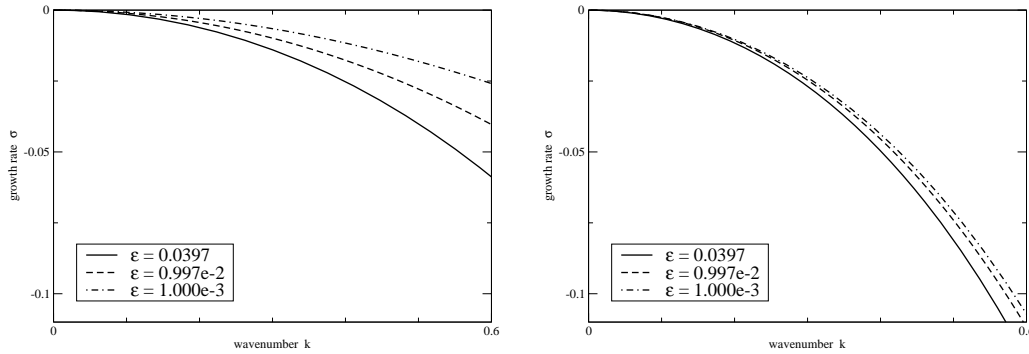

Figure 3: The (negative) growth rates for the (stable) zig-zag mode for different values of ε, for the no-slip case (left) and for the slip case (right).

6

3 Sharp-interface model for the slip-dominated case

3.1 Derivation of the model

Outer problem

We start from equation (1.3) for $n = 2$, i.e.,

$$h_t + \nabla \cdot \left[h^2 \nabla \cdot \left(\triangle h - \varepsilon^{-1} \Phi'\left(h/\varepsilon\right) \right) \right] = 0 \tag{3.1}$$

and the far-field conditions

$$\lim_{x \to \pm\infty} h(x, y, t) = \varepsilon h_\infty; \tag{3.2}$$

recall that h_∞ satisfies (2.3) and is of $O(1)$.

Transformation to inner coordinates near contact line

Let $\mathbf{x} = (x, y)$ be a point in the neighbourhood of the contact line, which we parametrize by $\mathbf{r}(t, s) = (r_1(t, s), r_2(t, s))$, where s denotes arclength. Then

$$\mathbf{x} = \mathbf{r}(t, s) + \varepsilon z \boldsymbol{\nu}(t, s) \tag{3.3}$$

defines the boundary layer with $z = O(1)$, which henceforth denotes the 'inner' variable. Note that for an infinite ridge we have two boundary layers, one on each side of the ridge, hence we have two parameter functions $\mathbf{r}(t, s)$ and two pairs of normal and tangent vectors. The normal vectors $\boldsymbol{\nu}(t, s) = (r_{2s}(t, s), -r_{1s}(t, s))$ point outside the ridge and the unit tangent vectors $\mathbf{t}(t, s) = (r_{1s}(t, s), r_{2s}(t, s))$ are oriented upwards, i.e. such that $r_{2s}(t, s) > 0$. In the inner region the height is much less than one, the appropriate scaling being

$$h = \varepsilon v. \tag{3.4}$$

Making use of appendix A we obtain the expression

$$\begin{aligned}
\nabla \cdot \left(h^2 \nabla p \right) \quad \sim \quad & \varepsilon^2 \left[2v \left(r_{1s}(1 - \varepsilon z \kappa)v_s + \varepsilon^{-1} r_{2s} v_z \right) \left(r_{1s}(1 - \varepsilon z \kappa)p_s + \varepsilon^{-1} r_{2s} p_z \right) \right. \\
& + 2v \left(r_{2s}(1 - \varepsilon z \kappa)v_s - \varepsilon^{-1} r_{1s} v_z \right) \left(r_{2s}(1 - \varepsilon z \kappa)p_s - \varepsilon^{-1} r_{1s} p_z \right) \\
& \left. + v^2 \left(\varepsilon^{-2} p_{zz} + \varepsilon^{-1} \kappa p_z + p_{ss} - z \kappa^2 p_z \right) \right]
\end{aligned} \tag{3.5}$$

where

$$p \sim -\varepsilon^{-1} v_{zz} - \kappa v_z - \varepsilon v_{ss} + \varepsilon z \kappa^2 v_z + \varepsilon^{-1} \Phi'(v) \qquad (3.6)$$

and κ is the curvature of the contact line. Hence, to leading order in ε the second term of (3.1) is

$$\varepsilon^{-1} \left[v^2 \left(v_{zz} - \Phi'(v) \right) \right]_z . \qquad (3.7)$$

Since the first term of (3.1) is transformed to

$$h_t \sim -\varepsilon V^{\mathbf{t}}(1 - \varepsilon z \kappa) v_s + V^{\boldsymbol{\nu}} v_z + \varepsilon v_t , \qquad (3.8)$$

where we denote the tangential and normal velocities by

$$V^{\mathbf{t}} = \mathbf{x}_t \cdot \mathbf{t} , \quad V^{\boldsymbol{\nu}} = \mathbf{x}_t \cdot \boldsymbol{\nu} , \qquad (3.9)$$

the leading order the inner problem becomes

$$\left[v^2 \left(v_{zz} - \Phi'(v) \right) \right]_z = 0 \qquad (3.10)$$

together with the boundary conditions

$$\lim_{z \to +\infty} v = 1, \ \lim_{z \to +\infty} v_z = 0, \ \lim_{z \to +\infty} v_{zz} = 0 . \qquad (3.11)$$

Integrating (3.11) twice, using the fact that the potential $\Phi'(1) = 0$, since Φ has a minimum there, we get $v_{zz} = \Phi'(v)$, hence

$$v_z = -2^{1/2} \left(\Phi(v) - \Phi(1) \right)^{1/2} . \qquad (3.12)$$

For matching we need the behavior for large z, which is

$$v_z \to -2^{1/2} \left(-\Phi(1) \right)^{1/2} \equiv -\lambda \quad \text{as} \quad z \to \infty. \qquad (3.13)$$

where the constant λ here corresponds to the macroscopic contact angle. For future reference, we remark that for the specific potential (1.2), the numerical value for λ is 0.8660. Transformation back to outer variables via

$$v \sim z\lambda , \quad \text{where} \quad z = \frac{(\mathbf{r} - \mathbf{x}) \cdot \boldsymbol{\nu}}{\varepsilon},$$

yields

$$h \sim (\mathbf{r} - \mathbf{x}) \cdot \boldsymbol{\nu} \, \lambda. \qquad (3.14)$$

8

The following sharp-interface model then results as the leading-order outer problem, together with the boundary condition found by matching to (3.14),

$$h_t = -\nabla \cdot (h^2 \nabla \triangle h) \quad \text{in} \quad \Omega, \tag{3.15}$$

$$\frac{\partial h}{\partial \nu} = -\lambda, \quad h = 0, \quad h^2 \frac{\partial}{\partial \nu} \triangle h = 0 \quad \text{on} \; \partial_1 \Omega = (s^-(y,t), y) \tag{3.16}$$

$$\frac{\partial h}{\partial \nu} = -\lambda, \quad h = 0, \quad h^2 \frac{\partial}{\partial \nu} \triangle h = 0 \quad \text{on} \; \partial_2 \Omega = (s^+(y,t), y), \tag{3.17}$$

where the third boundary condition in (3.16) and (3.17) arises by letting $z \to -\infty$, $v \to \infty$ in (3.10). The tangent and outward-normal vector along $\partial_1 \Omega$ are

$$\mathbf{t}^- = \frac{(s_y^-, 1)}{\sqrt{(s_y^-)^2 + 1}} \quad \text{and} \quad \boldsymbol{\nu}^- = \frac{(-1, s_y^-)}{\sqrt{(s_y^-)^2 + 1}}, \tag{3.18}$$

while along $\partial_2 \Omega$ they are

$$\mathbf{t}^+ = \frac{(s_y^+, 1)}{\sqrt{(s_y^+)^2 + 1}} \quad \text{and} \quad \boldsymbol{\nu}^+ = \frac{(1, -s_y^+)}{\sqrt{(s_y^+)^2 + 1}}. \tag{3.19}$$

3.2 Stationary-ridge solution

We now assume that the base state is not dependent of t and y, so that it is determined by the boundary value problem

$$(h^2 p_x)_x = 0, \quad \text{with} \quad p = -h_{xx}, \tag{3.20}$$

$$\frac{\partial h}{\partial \nu} = (h_x, 0) \cdot (-1, 0) = -h_x = -\lambda, \; h = 0, \quad h^2 h_{xxx} = 0 \quad \text{on} \; s^-, \tag{3.21}$$

$$\frac{\partial h}{\partial \nu} = (h_x, 0) \cdot (1, 0) = h_x = -\lambda, \quad h = 0, \quad h^2 h_{xxx} = 0 \quad \text{on} \; s^+. \tag{3.22}$$

Integrating (3.20) twice and using the third (mass-conservation) boundary conditions in (3.21) and (3.22) we find that $h_{xx} = -c$. Integrating this twice and using the first two boundary conditions in (3.21) and (3.22) we get

$$h = \frac{1}{2}c(x - s^-)(s^+ - x), \quad \text{and} \quad c(s^- - s^+) = -2\lambda. \tag{3.23}$$

Transforming the coordinate system again by setting $s^+ = s_0$ and $s^- = -s_0$, we obtain the base state in the simplified form

$$h_0 = \frac{1}{2}c(s_0^2 - x^2), \quad \text{and} \quad cs_0 = \lambda. \tag{3.24}$$

9

If we again normalize by choosing $\max h_0 = 1$ then we obtain

$$s_0 = \frac{2}{\lambda}, \quad \text{and} \quad c = \frac{\lambda^2}{2}. \tag{3.25}$$

3.3   Linear stability

We now investigate the linear stability of the base solution of the previous sub-section. Let

$$s^\pm = \pm s_0 + \beta s_1^\pm(y,t), \quad p = c + \beta p_1(x,y,t), \quad h = h_0 + \beta h_1(x,y,t). \tag{3.26}$$

At $O(\beta)$ we get

$$h_{1t} = (h_0^2 p_{1x})_x + h_0^2 p_{1yy} \quad \text{with} \quad p_1 = -h_{1xx} - h_{1yy} \tag{3.27}$$

and the boundary conditions

$$h_{1x} = \frac{\lambda^2}{2} s_1^\pm, \quad \text{at} \quad x = \pm s_0, \tag{3.28}$$

$$h_1 = \pm\lambda\, s_1^\pm, \quad \text{at} \quad x = \pm s_0, \tag{3.29}$$

$$h_0^2 h_{1xxx} = 0, \quad \text{at} \quad x = \pm s_0. \tag{3.30}$$

We make the usual ansatz

$$[\, s_1^\pm(y,t),\ p_1(x,y,t), h_1(x,y,t)\,] = [\,\hat{s}^\pm,\ \hat{p}(x),\ \hat{h}(x)\,]\, e^{\sigma t + iky} \tag{3.31}$$

and obtain from (3.27)-(3.30) and the variable transformation

$$\xi = \frac{\lambda}{2}\, x, \quad \tilde{k} = \frac{2}{\lambda}\, k, \quad \tilde{\sigma} = \frac{16}{\lambda^4}\, \sigma, \quad \tilde{s}_0 = \frac{\lambda}{2}\, s_0 \tag{3.32}$$

the eigenvalue problem

$$\tilde{\sigma}\hat{h} = -\left(h_0^2 \left(\hat{h}_{\xi\xi} - \tilde{k}^2 \hat{h} \right) \right)_{\xi\xi} + \tilde{k}^2 h_0^2 \left(\hat{h}_{\xi\xi} - \tilde{k}^2 \hat{h} \right) \tag{3.33}$$

$$\hat{h}_\xi = \pm\hat{h}, \quad \text{at} \quad \xi = \pm 1 \tag{3.34}$$

$$0 = h_0^2 \hat{h}_{\xi\xi\xi}, \quad \text{at} \quad \xi = \pm 1 \tag{3.35}$$

where

$$h_0 = 1 - \xi^2. \tag{3.36}$$

The ODE (3.33) has regular singular points at the boundary, i.e. at $\xi = \pm 1$. The formulation is symmetric in ξ, so the discussion of the behaviour of the general
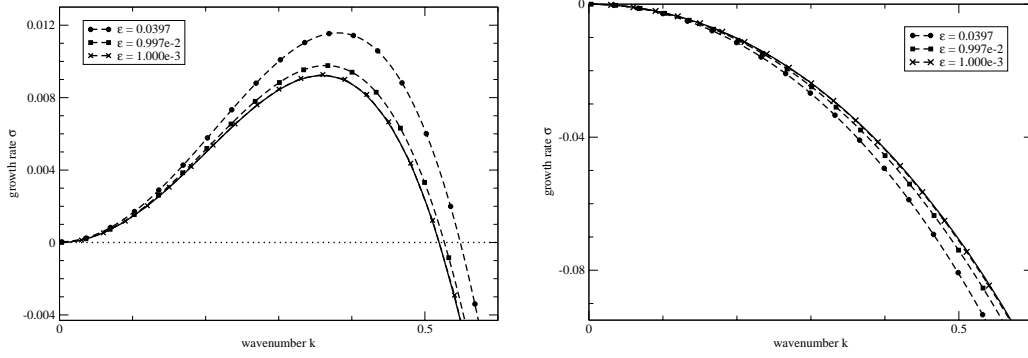
10

Figure 4: The top first eigenvalue (left figure) having even eigenfunction and the second eigenvalue (right figure) having odd eigenfunction, for the slip-dominated case. The results for the asymptotic model obtained from (3.32)-(3.36) are shown by a solid line, the results for the full model shown by dashed lines with symbols.

solution at $\xi = \pm 1$ can be done jointly for both points by setting $\zeta = \xi + 1$ and $\zeta = 1 - \xi$ for the left and right point respectively. This maps the boundary points to zero and yields the ODE (dropping the $\hat{\ }$'s and $\sim$'s)

$$
h_{\zeta\zeta\zeta\zeta} + \frac{4(1-\zeta)}{\zeta(2-\zeta)} h_{\zeta\zeta\zeta} - 2k^2 h_{\zeta\zeta} - k^2 \frac{4(1-\zeta)}{\zeta(2-\zeta)} h_\zeta
$$
$$
+ \left(\frac{\sigma}{\zeta^2(2-\zeta)^2} + k^2 \zeta^2 (2-\zeta)^2 \right) h = 0. \tag{3.37}
$$

The general solution is given by $h(\zeta) = \sum_{i=1}^4 C_i h_i(\zeta)$, where the expansions of the first two basis functions h_i are given at $\zeta = 0$ by the Taylor expansions

$$
h_1(\zeta) = \zeta^2 + O(\zeta^4), \quad h_2(\zeta) = \zeta + O(\zeta^3). \tag{3.38}
$$

The expansions for the remaining two basis functions are

$$
h_3(\zeta) = 1 + O(\zeta^6), \quad h_4(\zeta) = \zeta \ln(\zeta) + O(\zeta^2 \ln(\zeta)) \tag{3.39}
$$

if $\sigma = 0$, and

$$
h_3(\zeta) = 1 - \frac{\sigma}{8}\zeta^2 \ln(\zeta) + O(\zeta^3), \quad h_4(\zeta) = 1 - \frac{\sigma}{4}\zeta \ln(\zeta) + O(\zeta^3 \ln(\zeta)) \tag{3.40}
$$

otherwise. Note that here only h_3 in (3.39) is a Taylor expansion, while logarithms otherwise appear in the expansions for h_3 and h_4. In fact, h_4 is too singular to satisfy the boundary conditions (3.35), which in terms of ζ require $\zeta^2 h_{\zeta\zeta\zeta} \to 0$ at $\zeta \to 0$. Thus we must set $C_4 = 0$. The other boundary condition (3.34) requires

11

$h_\zeta + h \to 0$, from which we get the condition $C_2 + C_3 = 0$. In any case, this amounts to two conditions that are imposed on the general solution at each end of the interval, as required for a fourth-order boundary value problem.

We solved the eigenvalue problem (3.33)-(3.36), using a finite difference/vector iteration scheme, and compared the first two eigenvalues with those obtained for the full model in section 2, both being real for both models. The comparison is shown in figure 4, in terms of the wavenumber k and eigenvalue σ used in (3.31). It can be clearly seen that the eigenvalues for the full problem rapidly converge to the sharp-interface results as $\varepsilon \to 0$.

4 Sharp-interface model for the no-slip situation

4.1 Derivation of the model

Outer problem

We start from equation (1.3) for $n = 3$, i.e.

$$h_t + \nabla \cdot \left[h^3 \nabla \cdot \left(\triangle h - \varepsilon^{-1} \Phi'\left(h/\varepsilon \right) \right) \right] = 0 \tag{4.1}$$

and far-field conditions

$$\lim_{x \to \pm\infty} h(x, y, t) = \varepsilon h_\infty; \tag{4.2}$$

recall that h_∞ satisfies (2.3) and is of $O(1)$. To capture the instability we transform to the appropriate slow time scale via the logarithmic time dilatation

$$\tau = \delta t, \quad \delta := \frac{1}{\ln(1/\varepsilon)}. \tag{4.3}$$

Then (4.1) becomes

$$\delta h_\tau + \nabla \cdot \left[h^3 \nabla \cdot \left(\triangle h - \varepsilon^{-1} \Phi'\left(h/\varepsilon \right) \right) \right] = 0. \tag{4.4}$$

Note, that this can also be written as

$$\delta h_\tau - \nabla \cdot \left(h^3 \nabla p \right) = 0 \quad \text{where} \quad p = -\triangle h + \varepsilon^{-1} \Phi'\left(h/\varepsilon \right). \tag{4.5}$$

Transformation to inner coordinates near contact line

As in section 3 we let

$$\mathbf{x} = \mathbf{r}(\tau, s) + \varepsilon z \boldsymbol{\nu}(\tau, s) \qquad (4.6)$$

define the boundary layer with z being the 'inner' variable and set

$$h = \varepsilon v \qquad (4.7)$$

Making use again of appendix A we obtain the expression

$$
\begin{aligned}
\nabla \cdot \left(h^3 \nabla p \right) \quad \sim \quad & \varepsilon^3 \left[3v^2 \left(r_{1s}(1 - \varepsilon z \kappa) v_s + \varepsilon^{-1} r_{2s} v_z \right) \left(r_{1s}(1 - \varepsilon z \kappa) p_s + \varepsilon^{-1} r_{2s} p_z \right) \right. \\
& + 3v^2 \left(r_{2s}(1 - \varepsilon z \kappa) v_s - \varepsilon^{-1} r_{1s} v_z \right) \left(r_{2s}(1 - \varepsilon z \kappa) p_s - \varepsilon^{-1} r_{1s} p_z \right) \\
& \left. + v^3 \left(\varepsilon^{-2} p_{zz} + \varepsilon^{-1} \kappa p_z + p_{ss} - z \kappa^2 p_z \right) \right]
\end{aligned} \qquad (4.8)
$$

where p is given via appendix A, as in (3.6). The first term of (4.5) is transformed to

$$\delta h_\tau = -\varepsilon \delta V^{\mathbf{t}}(1 - \varepsilon z \kappa) v_s + \delta V^{\boldsymbol{\nu}} v_z + \varepsilon \delta v_\tau. \qquad (4.9)$$

Hence, to leading order, the inner problem reduces to

$$\left[v^3 (v_{zz} - \Phi'(v)) \right]_z = 0 \qquad (4.10)$$

with

$$\lim_{z \to \infty} v = 1, \ \lim_{z \to \infty} v_z = 0, \ \lim_{z \to \infty} v_{zz} = 0 \,.$$

As in section 3 we find

$$v_z = -2^{1/2} \left(\Phi(v) - \Phi(1) \right)^{1/2}, \qquad (4.11)$$

so that the slope is

$$v_z \to -\sqrt{-2\Phi(1)} = -\lambda \quad \text{for} \quad z \to -\infty. \qquad (4.12)$$

Higher order approximations for the slope may be found as demonstrated in appendix B.

Transition layer

In order to be able to match, we here need an additional transition layer. The layer that properly connects outer and inner layers is found by setting

$$\zeta = \delta V^{\boldsymbol{\nu}} \ln z, \quad v = z \, \varphi(\zeta), \qquad (4.13)$$

see [34] for details. Substitution of this into (4.8) and (4.9) we obtain the leading-order problem, assuming $1 - \zeta/V^{\nu} > 0$,

$$\varphi + \varphi^3 \varphi_\zeta = 0 \tag{4.14}$$

with solution

$$\varphi \sim (K - 3\zeta)^{1/3}. \tag{4.15}$$

Hence $\varphi = K^{1/3} + O(\zeta)$ for $\zeta \to 0$. Matching this to the solution of (4.11) using (4.12), we find that $K = \lambda^3$ and so

$$\varphi = (\lambda^3 - 3\zeta)^{1/3}. \tag{4.16}$$

Sharp-interface model

We can now derive a matching condition from (4.16) by transforming it back into the outer variables. From (4.13) we have

$$v = z \left(\lambda^3 - 3\,\delta V^{\nu} \ln z \right)^{1/3}, \quad \text{where} \quad z = \frac{(\mathbf{x} - \mathbf{r}) \cdot \boldsymbol{\nu}}{\varepsilon} \tag{4.17}$$

so that

$$h = (\mathbf{x} - \mathbf{r}) \cdot \boldsymbol{\nu} \, (\lambda^3 - 3V^{\nu})^{1/3} + O(\delta) \tag{4.18}$$

The following sharp-interface model then results as the leading-order outer problem, the boundary conditions being found by matching

$$\nabla \cdot (h^3 \nabla \triangle h) = 0 \qquad\qquad\qquad\qquad\quad \text{in } \Omega, \tag{4.19}$$

$$\frac{\partial h}{\partial \nu} = -(\lambda^3 + 3V^{\nu})^{1/3}, \quad h = 0, \quad h^3 \frac{\partial}{\partial \nu} \triangle h = 0 \quad \text{on } \partial_1 \Omega, \tag{4.20}$$

$$\frac{\partial h}{\partial \nu} = -(\lambda^3 + 3V^{\nu})^{1/3}, \quad h = 0, \quad h^3 \frac{\partial}{\partial \nu} \triangle h = 0 \quad \text{on } \partial_2 \Omega. \tag{4.21}$$

4.2   Stationary-ridge solutions and their linear stability

The stationary-ridge solutions of the sharp-interface model are the same as for the sharp-interface model for the slip case, i.e. parabolas with maximum normalized to one, and support $[-s_0, s_0]$, as stated in (3.24), (3.25). Now we again perturb these solutions, including the boundaries of the support, with normal-modes perturbations,

$$s^{\pm} = \pm s_0 + \beta s_1^{\pm}(k)\, e^{\hat{\sigma}\tau + iky}, \quad h = h_0 + \beta h_1(x; k)\, e^{\hat{\sigma}\tau + iky}, \tag{4.22}$$
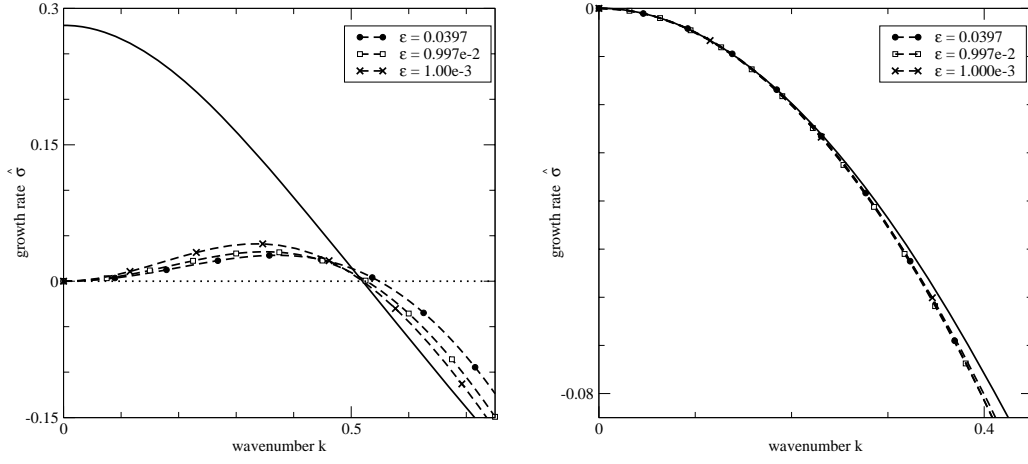
14

Figure 5: Here we show the dominant eigenvalue for the no-slip case (left figure) in outer scales (see (4.22) and (4.3)). The dashed lines with symbols show the results for the full model for different values of ε as indicated by the legend. The solid lines show the asymptotic results, using the eigenvalue $\hat{\sigma}_+$. The second (non-positive) eigenvalue for the no-slip case, in outer scales, compared to the asymptotic result $\hat{\sigma}_-$. The agreement of full and asymptotic model is quite good, in particular for longer wavelengths.

with $0 < \beta \ll 1$. Note that $\hat{\sigma}$ corresponds to the time variable τ, i.e. the relation to the growth rate in the scales of section 2 is $\sigma = \delta\hat{\sigma}$.

We then obtain to $O(\beta)$ the following eigenvalue problem, where $' = d/dx$,

$$h_1'' - k^2 h_1 = 0, \qquad \text{for} \quad -\frac{2}{\lambda} < x < \frac{2}{\lambda}, \tag{4.23}$$

$$h_1 \mp \lambda s_1^\pm = 0 \qquad \text{at} \quad x = \pm\frac{2}{\lambda}, \tag{4.24}$$

$$h_1' - \frac{1}{2}\lambda^2 s_1^\pm = -\frac{\hat{\sigma}}{\lambda^2} s_1^\pm \qquad \text{at} \quad x = \pm\frac{2}{\lambda}. \tag{4.25}$$

Note, that the eigenvalue appears only in the last boundary condition. The ODE (4.23) is easily solved and upon inserting the general solution into the boundary conditions one finds nontrivial solutions for h_1 and $s_1^\pm$ if $\hat{\sigma}$ is equal to one of the two values,

$$\hat{\sigma}_+ = \frac{1}{2}\lambda^3\left(\lambda - 2k\tanh(2k/\lambda)\right) \tag{4.26}$$

and

$$\hat{\sigma}_- = \frac{1}{2}\lambda^3\left(\lambda - 2k\coth(2k/\lambda)\right), \tag{4.27}$$

15

i.e. $\hat{\sigma}_\pm$ are the two eigenvalues. Note that for for shear-thickening liquids a similar asymptotic result was found in [31].

In figure 5 we compare the leading eigenvalues in outer scales from the numerical results for the full model by solving the eigenvalue problem (3.33)-(3.36) as before and comparing to the asymptotic values $\hat{\sigma}_+$ and $\hat{\sigma}_-$. Note here that the eigenvalues σ from section 2 have been rescaled appropriately with δ to match the scaling used for $\hat{\sigma}_\pm$. We find as $\varepsilon \to 0$ in figure 5 (right) that the numerical results approach the asymptotic value near the cut-off (neutrally stable) wavenumber k_c. In particular, the cut-off wavenumbers for the numerical results converge to the zero crossing of the asymptotic curve. In order to capture the linear stability behaviour for small wave numbers, we have to investigate the long-wave limit.

The long-wave limit

Consider a long wavelength perturbation of the ridge, so that the scales in the y-direction are much larger than in the x-direction, i.e. let $y = \hat{y}/\delta^{1/2}$. Hence, (4.5) is now

$$\delta h_\tau - (h^3 p_x)_x - \delta(h^3 p_{\hat{y}})_{\hat{y}} = 0, \quad \text{where} \quad p = -h_{xx} - \delta h_{yy} + \varepsilon^{-1}\Phi'(h/\varepsilon), \quad (4.28)$$

so that in this case to leading order

$$h^3 p_x = c(\hat{y}, \tau). \quad (4.29)$$

The boundary conditions $h^3 p_x = 0$ on $\partial_1 \Omega$ and $\partial_2 \Omega$ imply that $c(\hat{y}, \tau) = 0$ and $p = p(\hat{y}, \tau)$. Since, to leading order, $p = -h_{xx}$, integrating twice from s_- to s_+ yields the parabolic solution

$$h = -\frac{1}{2}p(\hat{y}, \tau)(x - s^-)(x - s^+). \quad (4.30)$$

Mass conservation leads to

$$\frac{\partial}{\partial \tau}\left(\int_{s_-}^{s^+} (x^2 - (s^- - s^+)x + s^- s^+) \, dx \, p\right) =$$
$$\frac{1}{4}\int_{s_-}^{s^+} \frac{\partial}{\partial \hat{y}}\left((x - s^-)^3(x - s^+)^3 p^3 \frac{\partial p}{\partial \hat{y}}\right) dx \quad (4.31)$$

and hence

$$\frac{\partial}{\partial \tau}\left[(s^+ - s^-)p\right] = \frac{3}{1120}\frac{\partial}{\partial \hat{y}}\left[(s^+ - s^-)^7 \frac{\partial p^4}{\partial \hat{y}}\right]. \quad (4.32)$$
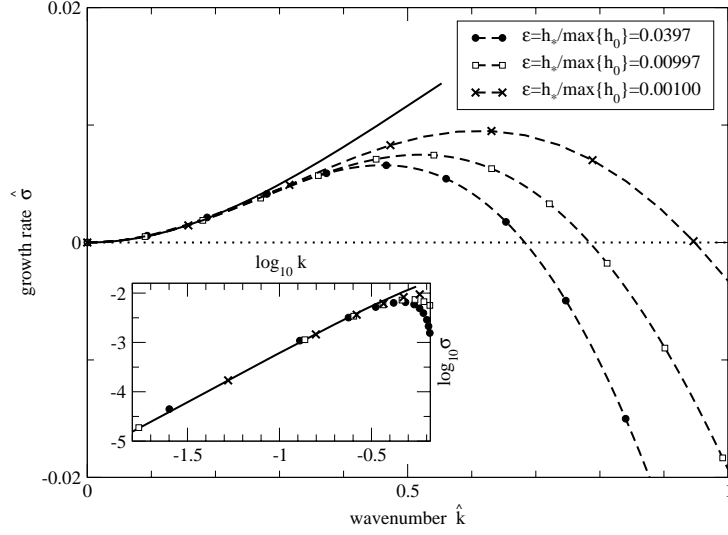
16

Figure 6: Here we show the dominant eigenvalue for the no-slip case and the larger solution of (4.47). Note that we show $\hat{\sigma}$, i.e. the eigenvalues are scaled as in figure 5, but the wavenumber is now in the scalings for the long-wave approximation, $\hat{k} = k/\delta^{1/2}$. The inset is a double logarithmic plot of part of the larger figure.

As the boundary conditions on (4.32) we find by matching to the inner solution that

$$s_\tau^\pm = \pm \frac{1}{3} \left(\mp h_x^3 - \lambda^3 \right).$$

Inserting (4.30) for h yields

$$s_\tau^\pm = \pm \frac{1}{3} \left(\frac{1}{8}(s^+ - s^-)^3 p^3 - \lambda^3 \right). \tag{4.33}$$

For the base state we note that $s^\pm$ and p are independent of y and t, and using (4.33), we get

$$h_0 = -\frac{1}{2} p_0 (x - s_0^-)(x - s_0^+), \quad p_0(s_0^+ - s_0^-) = 2\lambda. \tag{4.34}$$

If we put the origin in x-direction in the middle of the parabolic ridge, then $s_0^+ = s_0$ and $s_0^- = -s_0$ and

$$h_0 = -\frac{1}{2} p_0 (x^2 - s_0^2), \quad p_0 s_0 = \lambda. \tag{4.35}$$

Taking $\max h_0 = s_0^2 p_0 / 2 = 1$ yields the base state

$$s_0 = \frac{2}{\lambda}, \quad p_0 = \frac{\lambda^2}{2}. \tag{4.36}$$

17

Perturbation about this base state via

$$s^+ = s_0 + \beta s_1^+(\hat{y}, \tau) + O(\beta^2), \quad s^- = -s_0 + \beta s_1^-(\hat{y}, \tau) + O(\beta^2), \tag{4.37}$$

$$p = p_0 + \beta p_1(\hat{y}, t) + O(\beta^2), \tag{4.38}$$

yields at $O(\beta)$ the equations

$$s_0^2 p_0(s_1^+ - s_1^-)_\tau + s_0^3 p_{1\tau} = \frac{4}{35} s_0^7 p_0^3 p_{1\hat{y}\hat{y}}, \tag{4.39}$$

$$s_{1\tau}^\pm = \pm \left(p_0^2 s_0^3 p_1 + \frac{1}{2} p_0^3 s_0^2 (s_1^+ - s_1^-) \right). \tag{4.40}$$

A change of variable

$$s_1 := \frac{1}{2}(s_1^+ - s_1^-), \quad m_1 := \frac{1}{2}(s_1^+ + s_1^-) \tag{4.41}$$

simplifies the system to

$$3 s_0^2 p_0 s_{1\tau} + s_0^3 p_{1\tau} = \frac{6}{35} s_0^7 p_0^3 p_{1\hat{y}\hat{y}}, , \tag{4.42}$$

$$s_{1\tau} = p_0^2 s_0^3 p_1 + p_0^3 s_0^2 s_1, \tag{4.43}$$

$$m_{1\tau} = 0. \tag{4.44}$$

Hence using (4.36)

$$s_{1\tau} + \frac{4}{3\lambda} p_{1\tau} = \frac{16}{35} \frac{1}{\lambda} p_{1yy}, \quad s_{1\tau} = \lambda^2 \left(\frac{2}{\lambda} p_1 + \frac{\lambda^2}{2} s_1 \right). \tag{4.45}$$

The normal modes ansatz

$$s_1(\hat{y}, \tau) = a e^{\hat{\sigma}\tau + i\hat{k}\hat{y}} \quad \text{and} \quad p_1(\hat{y}, \tau) = b e^{\hat{\sigma}\tau + i\hat{k}\hat{y}} \tag{4.46}$$

yields then the following quadratic equation for the growth rate $\hat{\sigma}$

$$\hat{\sigma}^2 + \left(\lambda^4 + \frac{12}{35} \lambda^2 \hat{k}^2 \right) \hat{\sigma} - \frac{6}{35} \lambda^6 \hat{k}^2 = 0. \tag{4.47}$$

A comparison of the larger of the two solutions of (4.47) with the results for the full model in section 2 is shown in figure 6, in terms of $\hat{k}$ and $\hat{\sigma}$. Indeed, the agreement is good for small wave numbers and improves as ε is decreased. The other solution of (4.47) tends to a non-zero $O(1)$ for $k \to 0$, hence does not correspond to any of the two eigenvalues of the full problem we investigate here, which are both neutrally stable for $k = 0$.

18
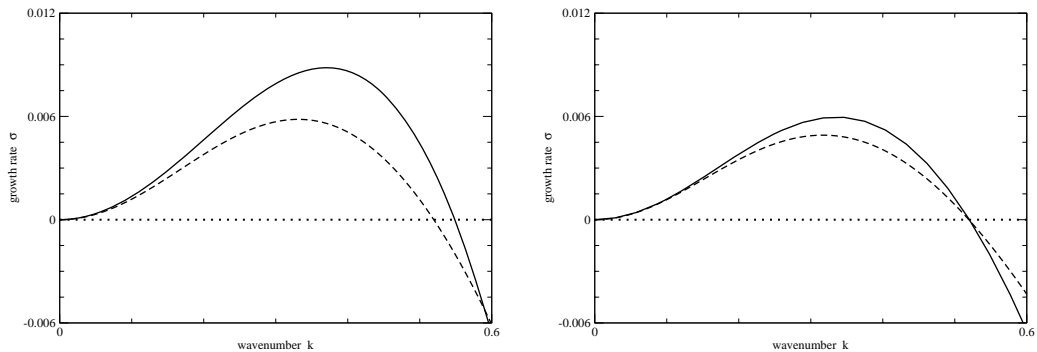
Figure 7: Her we compare the asymptotic composite solution (dashed line) to the eigenvalue problem for the full problem (3.33)-(3.36) (solid line) for $\varepsilon = 0.0397$ (left) and $\varepsilon = 1.000 \times 10^{-3}$ (right). The wavenumbers and growth rates are scaled as in section 2.

Composite solution

Finally, we can also compare the asymptotic composite solution with the solution to the eigenvalue problem for the full problem (3.33)-(3.36). For this we focus on the first eigenvalue. Equation (4.26) yields an approximation of $\sigma = \delta\hat{\sigma}$ for $k = O(1)$, while (4.47) is valid if $\hat{k} = O(1)$. Expanding the former at $k = 0$ yields

$$\sigma = \delta\hat{\sigma} \sim \delta \left(\frac{1}{2}\lambda^4 - 2\lambda^2 k^2 + \frac{8}{3}k^4 \right) \tag{4.48}$$

Expanding the solution of (4.47) at $\hat{k} = \infty$ we find after replacing $\hat{k}$ by $k/\delta^{1/2}$

$$\sigma = \delta\hat{\sigma} \sim \frac{1}{2}\delta\lambda^4 - \frac{35}{16}\delta\frac{\lambda^6}{k^2}. \tag{4.49}$$

Hence $\delta\lambda^4/2$ is the common part of both expansions. We therefore construct the composite solution by multiplying the solution of (4.47) (times δ) with the expression (4.26) (times δ) and then dividing by the common part. A comparison of this composite solution with our numerical results for the full model can be seen in figure 7.

5   Conclusion

In this paper we have derived sharp-interface models for a stationary ridge from the lubrication models with mobilities h^3 and h^2, corresponding to the no-slip

boundary condition at the liquid/solid interface and an intermediate slip condition, respectively. For this simple situation we were able to derive, in the no-slip case, analytical expressions for the dispersion relations that characterize the linear stability of the three-phase contact line. The instability mechanism is closely related to Rayleigh-Plateau instability of a free cylinder of fluid – as the peristaltic pertubations grow, the ridge can be expected to break up and eventually form droplets with circular contact lines in order to reduce its surface area. Our approach can be generalized to the situation of a dewetting ridge, the major differences being that the base state is not stationary and non-symmetrical due to the non-symmetrical form of the boundary conditions.

Acknowledgements

Appendix A

Transformation to inner variables

For completeness we include here the transformation formulae for the innere region.

Suppose $\tilde{w}$ is a quantity defined in the inner coordinates (s, z, τ). Then its derivatives are related to the derivatives of the corresponding quantity w in outer coordinates via the invertible transformation matrix

$$M = \begin{pmatrix} & & 0 \\ Q & & 0 \\ x_\tau & y_\tau & 1 \end{pmatrix}, \quad \text{where} \quad Q = \begin{pmatrix} x_s & y_s \\ x_z & y_z \end{pmatrix}, \tag{A.1}$$

by

$$\begin{pmatrix} \tilde{w}_s \\ \tilde{w}_z \\ \tilde{w}_\tau \end{pmatrix} = M \begin{pmatrix} w_x \\ w_y \\ w_\tau \end{pmatrix}. \tag{A.2}$$

Since s is arclength, we have

$$r_{1s}^2 + r_{2s}^2 = 1\,, \quad r_{1s}r_{1ss} + r_{2s}r_{2ss} = 0\,, \quad \kappa(s,\tau) = r_{1s}r_{2ss} - r_{2s}r_{1ss} \qquad \text{(A.3)}$$

and the (two-dimensional) Frenet-Serret formulae

$$\mathbf{t}_s = \kappa\boldsymbol{\nu}\,, \quad \boldsymbol{\nu}_s = -\kappa\mathbf{t}\,, \qquad \text{(A.4)}$$

so that

$$r_{1ss} = -\kappa r_{2s}\,, \quad r_{2ss} = \kappa r_{1s}\,. \qquad \text{(A.5)}$$

Hence

$$\mathbf{x}_s = (1 - \varepsilon\, z\, \kappa)\mathbf{t}\,, \quad \mathbf{x}_z = \varepsilon\boldsymbol{\nu}\,, \quad \det Q = \varepsilon(1 - \varepsilon\, z\, \kappa)\,. \qquad \text{(A.6)}$$

Now we can express the derivatives with respect to the outer variables of a quantity w in terms of the inner variables by

$$
\begin{pmatrix} w_x \\ w_y \\ w_\tau \end{pmatrix} = \begin{pmatrix} & & 0 \\ & Q^{-1} & 0 \\ -\mathbf{x}_\tau \cdot Q^{-1} & & 1 \end{pmatrix} \begin{pmatrix} \tilde{w}_s \\ \tilde{w}_z \\ \tilde{w}_\tau \end{pmatrix}
$$

$$
\sim \begin{pmatrix} r_{1s}(1 + \varepsilon z\kappa) & -\varepsilon^{-1}r_{2s} & 0 \\ r_{2s}(1 + \varepsilon z\kappa) & \varepsilon^{-1}r_{1s} & 0 \\ -V^{\mathbf{t}}(1 + \varepsilon z\kappa) & -\varepsilon^{-1}V^{\boldsymbol{\nu}} & 1 \end{pmatrix} \begin{pmatrix} \tilde{w}_s \\ \tilde{w}_z \\ \tilde{w}_\tau \end{pmatrix} \qquad \text{(A.7)}
$$

as $\varepsilon \to 0$, where we have used the approximation $1/(1 - \varepsilon z\kappa) = 1 + \varepsilon z\kappa + O(\varepsilon^2)$.

The second derivatives then transform as follows:

$$
\begin{aligned}
w_{xx} &\sim \varepsilon^{-2}r_{2s}^2\tilde{w}_{zz} - \varepsilon^{-1}\left[\kappa r_{1s}^2\tilde{w}_z + 2r_{1s}r_{2s}\tilde{w}_{sz}\right] + r_{1s}^2\tilde{w}_{ss} \\
&\quad -2\kappa r_{1s}r_{2s}\tilde{w}_s - z\kappa\left[\kappa r_{1s}^2\tilde{w}_z + 2r_{1s}r_{2s}\tilde{w}_{sz}\right] \qquad \text{(A.8)}
\end{aligned}
$$

$$
\begin{aligned}
w_{yy} &\sim \varepsilon^{-2}r_{1s}^2\tilde{w}_{zz} - \varepsilon^{-1}\left[\kappa r_{2s}^2\tilde{w}_z - 2r_{1s}r_{2s}\tilde{w}_{sz}\right] + r_{2s}^2\tilde{w}_{ss} \\
&\quad +2\kappa r_{1s}r_{2s}\tilde{w}_s - z\kappa\left[\kappa r_{2s}^2\tilde{w}_z - 2r_{1s}r_{2s}\tilde{w}_{sz}\right] \qquad \text{(A.9)}
\end{aligned}
$$

$$
\begin{aligned}
w_{xy} &\sim -\varepsilon^{-2}r_{1s}r_{2s}\tilde{w}_{zz} - \varepsilon^{-1}\left[\kappa r_{1s}r_{2s}\tilde{w}_z + \left(r_{2s}^2 - r_{1s}^2\right)\tilde{w}_{sz}\right] \\
&\quad +r_{1s}r_{2s}\tilde{w}_{ss} - \kappa\left(r_{2s}^2 - r_{1s}^2\right)\tilde{w}_s \\
&\quad -z\kappa\left[\kappa r_{1s}r_{2s}\tilde{w}_z + \left(r_{2s}^2 - r_{1s}^2\right)\tilde{w}_{sz}\right] \qquad \text{(A.10)}
\end{aligned}
$$

$$
\triangle w \sim \varepsilon^{-2}\tilde{w}_{zz} - \varepsilon^{-1}\kappa\tilde{w}_z + \tilde{w}_{ss} - z\kappa^2\tilde{w}_z \qquad \text{(A.11)}
$$

Appendix B

Higher order approximation for the slope

Higher order in δ approximations for λ (the slope used in the main part of the paper will be denoted here by λ_0) may be achieved by starting with the equation (4.4)

$$\delta h_\tau + \nabla \cdot \left(h^3 \nabla \cdot \left[\triangle h - \varepsilon^{-1} \Phi'(h/\varepsilon) \right] \right) = 0. \tag{B.1}$$

In inner scales, keeping $O(\delta)$ terms, we obtain with $h = \varepsilon g$

$$\delta \dot{s} g_z \sim \left(g^3 \left(g_{zz} - \Phi'(g) \right)_z \right)_z . \tag{B.2}$$

Integrating yields

$$\delta \dot{s}(g - h_\infty) \sim g^3 \left(g_{zz} - \Phi'(g) \right)_z , \quad \text{where} \quad h_\infty \sim 1. \tag{B.3}$$

Let $g \sim g_0 + \delta g_1$, then to leading order in δ we find

$$\frac{1}{2} g_{0z}^2 = \Phi(g_0) - \Phi(1), \quad \text{so that} \quad \lambda_0 = \sqrt{2(-\Phi(1))}, \tag{B.4}$$

or, if we set

$$g_{0z} = -\Psi(g_0), \quad \text{we find} \quad \lambda_0 = \Psi(\infty). \tag{B.5}$$

To next order we get

$$\dot{s}(g_0 - 1) = g_0^3 \left(g_{1zz} - \Phi''(g_0) g_1 \right)_z . \tag{B.6}$$

Integrating this yields

$$g_{1zz} - \Phi''(g_0) g_1 = \dot{s} \int_{-\infty}^z \frac{g_0 - 1}{g_0^3} dz = \dot{s} \int_{g_0}^\infty \frac{g - 1}{g^3 \Psi(g)} dg \tag{B.7}$$

If we denote

$$\Omega(g_0) = \int_{g_0}^\infty \frac{g - 1}{g^3 \Psi(g)} dg , \tag{B.8}$$

then, making use of (B.4), we obtain the equation

$$g_{0z} g_{1zz} - g_1 g_{0zzz} = \dot{s} \Omega(g_0) g_{0z} \tag{B.9}$$

Integrating once we find

$$g_{0z} g_{1z} - g_1 g_{0zz} = -\dot{s} \int_z^\infty \Omega(g_0) g_{0z} dz = \dot{s} \int_1^{g_0} \Omega(g) \, dg. \tag{B.10}$$

22

Thus

$$-\lambda_0 g_{1z} = \dot{s} \int_1^\infty \Omega(g)\, dg \quad \text{as} \quad z \to -\infty. \tag{B.11}$$

If we now let $\lambda \sim \lambda_0 + \delta\lambda_1$, then we find

$$\lambda_1 = \frac{\dot{s}}{\lambda_0} \int_1^\infty \Omega(g)\, dg\,. \tag{B.12}$$

Better comparison with the numerical solutions can now be obtained by replacing λ by $\lambda_0 + \delta\lambda_1$.

References

[1] H. Huppert. Flow and instability of a viscous current down a slope. *Nature*, 300:427–429, 1982.

[2] N. Silvi and E.B. Dussan V. On the rewetting of an inclined solid surface by a liquid. *Phys. Fluids*, 28:5–7, 1985.

[3] A. L. Bertozzi and M. P. Brenner. Linear stability and transient growth in driven contact lines. *Phys. Fluids*, 9:530–539, 1997.

[4] S. M. Troian, E. Herbolzheimer, S. A. Safran, and J. F. Joanny. Fingering instabilities of driven spreading films. *Europhys. Lett.*, 10:25–30, 1989.

[5] A. M. Cazabat, F. Heslot, S. M. Troian, and P. Carles. Finger instability of thin spreading films driven by temperature gradients. *Nature*, 346:824–826, 1990.

[6] J. B. Brzoska, F. Brochard-Wyart, and F.B. Rondelez. Exponential growth of fingering intabilities of spreading films under horizontal thermal gradients. *Europhys. Lett.*, 19:97–102, 1992.

[7] N. Garnier, R. O. Grigoriev, and M. F. Schatz. Optical manipulation of microscale fluid flow. *Phys. Rev. Lett.*, 91:Art.–No. 054501, 2003.

[8] D. E. Kataoka and S. M. Troian. A theoretical study of instabilities at the advancing front of thermally driven coating films. *J. Coll. Int. Sci.*, 192:350–362, 1997.

[9] A. L. Bertozzi, A. Münch, X. Fanton, and A. M. Cazabat. Contact line stability and 'undercompressive shocks' in driven thin film flow. *Phys. Rev. Lett.*, 81:5169–5172, 1998.

[10] P. G. López, S. G. Bankoff, and M. J. Miksis. Non-isothermal spreading of a thin liquid film on an inclined plane. *J. Fluid Mech.*, 11:1–39, 1996.

[11] A. Münch and B. A. Wagner. Numerical and asymptotic results on the linear stability of a thin film spreading down a slope of small inclination. *Euro. J. Appl. Math.*, 10:297–318, 1999.

[12] R. Seemann, S. Herminghaus, and K. Jacobs. Dewetting patterns and molecular forces: A reconciliation. *Phys. Rev. Lett.*, 86:5534–5537, 2001.

[13] R. Seemann, S. Herminghaus, and K. Jacobs. Gaining control of pattern formation of dewetting films. *J. Phys.: Condensed Matter*, 13:4925–4938, 2001.

[14] Rahul Konnur, Kajari Kargupta, and Ashutosh Sharma. Instability and morphology of thin liquid films on chemically heterogeneous substrates. *Phys. Rev. Lett.*, 84:931–934, 2000.

[15] G. Reiter. Dewetting of thin polymer films. *Phys. Rev. Lett.*, 68:75–78, 1992.

[16] Günter Reiter, Ashutosh Sharma, Alain Casoli, Marie-Odile David, Rajesh Khanna, and Philippe Auroy. Thin film instability induced by long-range forces. *Langmuir*, 15:2551–2558, 1999.

[17] Ashutosh Sharma and Rajesh Khanna. Pattern formation in unstabile thin liquid films. *Phys. Rev. Lett.*, 81:3463–3466, 1998.

[18] Ashutosh Sharma and Rajesh Khanna. Pattern formation in unstable thin liquid films under influence of antagonistic short- and long-range forces. *Journal of Chemical Physics*, 110:4929–4936, 1999.

[19] R. Xie, A. Karim, J. F. Douglas, C. C. Han, and R. A. Weiss. Spinodal dewetting of thin polymer films. *Phys. Rev. Lett.*, 81:1251–1254, 1998.

[20] C. Neto and K. Jacobs. Dynamics of hole growth in dewetting polystyrene films. *Physica A*, 339:66–71, 2004.

24

[21] A. Sharma and G. Reiter. Instability of thin polymer films on coated substrates: Rupture, dewetting and drop formation. *J. Coll. Int. Sci.*, 178:383–389, 1996.

[22] G. Reiter and A. Sharma. Auto-optimization of dewetting rates by rim instabilities in slipping polymer films. *Phys. Rev. Lett.*, 80, 2001.

[23] J.-L. Masson, O. Olufokunbi, and P. F. Green. Flow instabilities in entangled polymer films. *Macromolecules*, 35:6992–6996, 2002.

[24] A. Münch and B. Wagner. Contact-line instability of dewetting thin films. Accepted: Physica D, 2004.

[25] A. Münch, B. Wagner, and T.P. Witelski. Lubrication models for small to large slip-lengths. Accepted: J. Engr. Math., 2005.

[26] C. Redon, F. Brochard-Wyart, and F. Rondelez. Dynamics of dewetting. *Phys. Rev. Lett.*, 66:715–718, 1991.

[27] F. Brochard-Wyart, P.-G. de Gennes, H. Hervert, and C. Redon. Wetting and slippage of polymer melts on semi-ideal surfaces. *Langmuir*, 10:1566–1572, 1994.

[28] K. Jacobs, R. Seemann, G. Schatz, and S. Herminghaus. Growth of holes in liquid films with partial slippage. *Langmuir*, 14:4961–4963, 1998.

[29] A. Oron, S. H. Davis, and S. G. Bankoff. Long-scale evolution of thin liquid films. *Rev. Mod. Phys.*, 69:931–980, 1997.

[30] A. Münch. Dewetting rates of thin liquid films. MATHEON preprint number 123, 2004.

[31] J. C. Flitton and J. R. King. Surface-tension-driven dewetting of Newtonian and power-law fluids. *J. Engr. Math.*, 50:241–266, 2005.

[32] K. B. Glasner. Variational models for moving contact lines and the quasi-static approximation. Preprint, 2004.

[33] K. B. Glasner. A boundary integral formulation of quasi-steady fluid wetting. Preprint, 2004.

[34] J. R. King. The spreading of power law fluids. In A. C. King and Y. D. Shikmurzaev, editors, *Proc. of the IUTAM Symposium on Free Surface Flows*, pages 153–160, Dordrecht, 2001. Kluwer.